Pol. J. Environ. Stud. Vol. 31, No. 5 (2022), 4117-4125
DOI: *10.15244/pjoes/147023* ONLINE PUBLICATION DATE: 2022-05-20

Original Research

Photocatalytic Performance of TiO_2-ZnAl LDH Based Materials: Kinetics and Neural Networks Approach

Milica Hadnadjev-Kostic*, Tatjana Vulić, Nataša Lukić, Aleksandar Jokić, Djurdjica Karanovic

University of Novi Sad, Faculty of Technology Novi Sad, Bul. cara Lazara 1, Novi Sad, Serbia

Received: 22 December 2021
Accepted: 1 March 2022

Abstract

Photodegradation of azo dyes from industrial wastewater is challenging due to their high stability and resistance to removal. In this study, a generalized predictive model for photodegradation behavior of TiO_2 containing ZnAl layered double hydroxide (LDH) based materials in the removal process of cationic azo dyes (Rhodamine B and Methylene Blue) was proposed. The performed kinetic investigation suggested good correlation of the experimental results with theoretical settings and revealed that all photocatalysts in both photocatalytic removal reactions followed the pseudo-first order Langmuir-Hinshelwood reaction model. The inputs for artificial neural network (ANN) included four experimental variables: TiO_2 loading onto LDHs, organic dye type used for the removal process, temperature of thermal treatment of photocatalysts and reaction time, whereas for the two ANN prediction outputs removal efficiency and photo-degradation rate constants were used. The optimal topology was determined to be a three-layer feed-forward ANN with 3 input neurons and 10 hidden neurons, 3-10-1.

Keywords: heterogeneous photocatalysis, TiO_2-loading, methylene blue and Rhodamin B photodegradation, pseudo first-order kinetics, reaction rate constant, Artificial Neural Network, water treatment, model validation

Introduction

Over the past few years, due to large-scale industrialization water pollution has considerably increased in ecosystems and has become a rising aquatic environmental problem. The use of organic dyes in different industries lead to substantial amounts of colored wastewater [1]. It has been stated in the literature that 70% of these dyes impose as complex synthetic, hazardous azo structures and around 12-15% are discharged into the environment untreated causing severe threat to human health and environmental safety [2]. Rhodamine B (RhB) and Methylene Blue (MB) are the most frequently used dyes in paper, plastic, textile industries and can have mutagenic and toxic properties impacting the environment causing serious acute and chronic health issues in living organisms

*e-mail: hadnadjev@tf.uns.ac.rs

[3]. Considering the rapid pollution increase, there is a growing demand for non-conventional processes that ensure the energy efficient purification of polluted water. Heterogeneous photocatalytic oxidation that involves free-radical reactions initiated by light irradiation of the photocatalysts' surface is one of the promising purification methods [4, 5]. These photocatalytic semiconductors can operate under specific light spectrum range and their efficiency depend predominately on the electron-hole pairs' mobility and on the accessibility of active sites, but is additionally influenced by other numerous factors [6, 7].

Titanium dioxide (TiO_2) has been widely used as a photocatalyst due to its high oxidative power, photo-stability and non-toxicity. Considering that TiO_2 photocatalyic efficiency depends on crystal structure, particle size and surface area, nano-sized TiO_2, therefore has enhanced efficiency initiated by UV light, but due to inhalation toxicity and possible nanoparticle aggregation their application should be reduced [8]. In order to prevent the mentioned aggregation and inhalation, these nanoparticles could be loaded onto appropriate support.

As environmental-friendly materials, used as both photocatalysts and photocatalyst support, layered double hydroxides (LDHs), also known as a class of synthetic two-dimensional nanostructured anionic clays, have been investigated. The general formula is $[M(II)_{1-x}M(III)_x(OH)_2]_x+(A_{n-x/n})\cdot mH_2O$, where M(II) and M(III) are divalent and trivalent cations, A_{n-} the interlayer anions, x the ratio between M(III) and total metal amount (M(III) + M(II)) [9]. After thermal treatment, the layered structure of these materials collapses forming non-stoichiometric metastable mixed oxides with developed surface area and specific acid-base and redox properties [10, 11].

The photocatalytic performance of materials depends on several important experimental variables (catalysts dosage, temperature of the thermal treatment, initial concentration of the contaminant, reaction time etc.). Even though data regarding various methods is available, there is a lack of standard characterization that complicates the reproduction and the comparison of reported data [12]. Considering that degradation mechanism by photocatalytic route is a quite complex phenomena and requires many sets of degradation experiments to optimize the dosage of catalyst and the pollutant concentration, reaction mechanisms, as well as the effect of operational parameters on the reaction is very difficult to define. Due to the complex nature of photocatalytic degradation processes and many experimental variables that influence the degradation efficiency in the experimental design, it is difficult to model these processes using traditional methods. Therefore, there is an ongoing search for an alternative well-adjusted model that would enable better comprehension, labor reduction and system identification.

Artificial neural network (ANN) model is a suitable way to predict experimental trends in various systems, especially for catalytic processes since it is a promising tool because of the simplicity in simulation and prediction. Moreover, ANN has the ability to self-learn, self-organize, adapt, and has good nonlinear mapping. Therefore, through ANN, modeling and optimization can be achieved [13]. Considering the ANN advantages regarding the reduced time requirement for the development of the model than traditional mathematical models, this model has recently been applied in engineering and science [14]. The model is based on biological neural systems with an interconnection of functions and variables that are revealed in three main layers of neurons (input, hidden and output layers) which are adjusted with their weights and biases [15]. Besides the numerous advantages of the ANN model, this model can successfully be employed to simulate the process and define the significance of the various operating variables [16, 17].

In this present work, we propose a generalized predictive model for photodegradation behavior of a series of TiO_2 containing ZnAl LDHs in the removal process of cationic azo dyes (Rhodamine B and Methylene Blue) using ANN modeling. The required dataset were collected from our publications and from the presented kinetic studies. The inputs for ANN included four experimental variables: TiO_2 loading onto LDH, organic dye type (ODT), temperature of thermal treatment and reaction time, which basically covered all the experimental conditions. The two prediction outputs of ANN were removal efficiency and photo-degradation rate constants of the organic contaminants.

Experimental

Synthesis of Photocatalysts

Zn-Al layered double hydroxide with carbonate anions in the interlayer was synthesized by low supersaturation coprecipitation method at constant pH (9-9.5) and temperature (40ºC). The precipitates were aged (15 h), dried at 100ºC (24 h) and then calcined for 5 h, at 500ºC in air. These dried samples were denoted as 0%-100ºC and calcined as 0%-500ºC (samples without TiO_2 loading). Furthermore wet impregnation of TiO_2 (VP Disp. W 2730 X Degussa) onto calcined ZnAl-LDHs was utilized for the preparation of TiO_2-ZnAl LDH based photocatalysts where the TiO_2-loading varied (1 mass%, 2 mass% and 3 mass%). These impregnated samples were dried at 100ºC for 12 h and designated as 1%-100ºC, 2%-100ºC and 3%-100ºC depending on the TiO_2 dosage, whereas after calcination (5h, at 500ºC in air) the obtained samples were denoted as 1%-500ºC, 2%-500ºC and 3%-500ºC. The TiO_2-samples without loading on ZnAl-LDH were also dried (100%-100ºC) and calcined (100%-500ºC). Detailed synthesis and preparation steps are presented in our previous published study [4, 8, 18].

Photocatalytic Degradation of Methylene Blue and Rhodamine B

The photocatalytic efficiency of MB and RhB degradation was studied for all synthesized and calcined samples in aqueous solution under UV-A light (Osram Eversun L40 W/79 K lamp) in an open cylindrical thermostated Pyrex reaction vessel. Before illumination, the reaction mixtures, 50 mg of catalysts and 100 ml of MB/RhB water solution (10 μmol/l), were stirred in the dark for 30 minutes to ensure adsorption/desorption equilibrium between the dye and the catalyst surface. The reaction solutions with the catalyst powder were stirred and analyzed at predetermined time intervals. In order to eliminate the influence of possible adsorption phenomena, blank samples - reaction solutions with catalysts, were kept in the dark and treated the same way as irradiated samples.

The photocatalytic efficiency of ODT degradation, E, was calculated based on total conversion using the formula:

$$E = \frac{[C_0 - C]}{C_0} \times 100\ (\%) \tag{1}$$

where C_0 was the ODT concentration in blank sample and C the ODT concentration in irradiated samples, measured at defined time intervals. The ODT concentration was measured by UV-VIS spectrophotometry (EVOLUTION 600 spectrophotometer) at λ = 554 nm for RhB and at λ = 664 nm for MB.

Kinetic Models

The photodegradation of ODT is commonly defined by the pseudo first-order reaction that follows the Langmuir-Hinshelwood (L-H) kinetic model [19, 20].

$$r_i = -\frac{dC_i}{dt} = k_{app} \times C_i \tag{2}$$

where r_i is the reaction rate, t is the irradiation time, C_i is the concentration of the substrate and k_{app} is the observed apparent first-order photodegradation rate constant.

Considering that C_i is the ODT concentration, after the integration of the previous equation (2), the model can be expressed by the following equation:

$$ln\left(\frac{[ODT]_0}{[ODT]_t}\right) = k_p \times t \tag{3}$$

where $[ODT]_t$ and $[ODT]_0$ is the RhB or MB concentration at defined time periods, t (min). Since this can be presented as linear function with $ln([ODT]_0/[ODT]_t)$ vs. t, the k_{app} can be determined from the slope. In this study the Langmuir-Hinshelwood model was used to describe the reaction kinetics for the photocatalytic degradation occurring at the solid-liquid surface, as well as to determine the relationship of the apparent first-order rate constant and the initial ODT concentration.

Artificial Neural Network Architecture

The artificial network data sets were normalized to bring all data within a specific range [21]:

$$Y_{norm} = (1 - \Delta^L - \Delta^U) \cdot \frac{Y - Y_{min}}{Y_{max} - Y_{min}} + \Delta^L \tag{4}$$

where: Y_{norm} and Y, are the normalized and measured values of efficiency or calculated values of reaction constant, whilst Y_{min} and Y_{max} are minimum and maximum values in data sets, respectively; Δ^L and Δ^U are the lower and upper limits for the normalization (with values of 0.01 for each limit).

The multi-layer feed-forward with backpropagation neural networks are the most popular and most widely used models in many practical applications especially for functional fitting. [22]. In this study the Levenberg-Marquardt (LM) training algorithm is selected due to its convergence rate and the performance of the network in seeking a optimal solution. The Lavenberg-Marquardt algorithm uses an early stopping criterion to improve network training speed and efficiency.

The data are divided into three randomized sets. The division of the dataset in the research work is 70% for the training data, 15% for the validation data, and 15% for the testing data. The training set is for determining the weights and biases of the network. The validation data set is for evaluating the weights and biases and for deciding when to stop training. The validation error generally decreases at the beginning of the training process, but when the network starts to over-fit the data, the validation error begins to increase. The training is stopped when the validation error begins to increase and the weights and biases will then be derived at the minimum error. A maximum validation failure is set to default value of five epochs [23]. The last data set is for testing, the weights and biases are used to verify the capability of the stopping criterion and to estimate the expected network operation on new data sets. The randomization algorithm used, is built in Matlab function 'randperm'.

Internal ANN features such as the number of hidden layers, the number of neurons in each layer, momentum factor, learning rate, transfer functions, and initial weight distribution have great impact on ANN model building. Default values were selected for some of these factors (momentum factor and learning rate), since they only affect the training time [24]. In our study, the maximum number of epochs, target error goal MSE (mean square error), and minimum performance gradient are set to 1500, 0, and 10^{-10}, respectively.

Training stops when the maximum number of epochs is reached or when either the MSE or performance gradient is minimized to reach at the predetermined goal.

Number of neurons in the hidden layer is critical for ANN model performance [25]. The small number of hidden neurons causes that the ANN is unable to predict experimental data precisely, whereas when the number of hidden neurons is too big the over-fitting problem may occur. Moreover, too many neurons do not propagate errors back efficiently [25] and therefore worsen the ability of the neural network to learn. A trial and error based method was selected for determining the number of neurons in the hidden layer.

Neurons in network layer are connected by different activation functions. The connection of hidden layer neurons to output layer was linear (purelin). In the case of input neurons connections to the hidden, two types of activation functions are examined i.e. log-sigmoid (logsig) or hyperbolic tangent sigmoid (tansig).

The performance is calculated using the mean-squared-error (MSE) and coefficient of determination, R^2, according to Eqs. (5) and (6):

$$R^2 = 1 - \frac{\sum_{i=1}^{n}\left(Y_{exp,i} - Y_{pred,i}\right)^2}{\sum_{i=1}^{n}\left(Y_{exp,i} - Y_{pred,avg}\right)^2} \quad (5)$$

$$MSE = \frac{1}{n}\sum_{i=1}^{n}\left(Y_{exp,i} - Y_{pred,i}\right)^2 \quad (6)$$

where: n is the number of data points, $Y_{exp,i}$ and $Y_{pred,i}$ are the normalized experimental and predicted values obtained from the experiments and neural network model, respectively and $Y_{pred,avg}$ is the average of the predicted values.

Two ANN models were generated for efficiency of ODT degradation and photodegradation rate constant. The input layer for the first network consists of four neurons i.e. organic dye type (ODT), TiO_2-loading onto LDH, temperature of thermal treatment and reaction time, while the output layer has one neuron efficiency of ODT degradation. The second neural network was used for photodegradation rate constant prediction (output), whilst inputs were organic dye type (ODT), TiO_2-loading onto LDH and temperature of thermal treatment. The ANN predictive model simulations were carried out using mathematical software Matlab R2015b.

Since the neural network is highly dependent upon the initial weights values and in order to achieve the best results, the neural networks were run 50 times and the average values of statistical indicators (MSE and R^2), were used for comparing network performances [26].

ANN should not simply be used as black box model, since cause-effect information can be quantitatively extracted from network connection weights to assist in model development and experimental design [23]. Relative importance (RI) of input variable is calculated according to the following equation:

$$RI = \frac{\sum_{j=1}^{n_H}\left[\left(i_{vj}/\sum_{k=1}^{n_v} i_{kj}\right)O_j\right]}{\sum_{i=1}^{n_v}\left[\sum_{j=1}^{n_H}\left(\left(i_{vj}/\sum_{k=1}^{n_v} i_{kj}\right)O_j\right)\right]} \quad (7)$$

where: n_v is the number of input neurons, n_H the number of hidden neurons, i_{vj} the absolute value of connection weights between the input and hidden layers, and O_j is the absolute value of connection weights between the hidden and output layers.

Results and Discussion

Kinetic Studies

Considering that the Langmuir-Hinshelwood (L-H) model the photocatalytic reaction is described as the reaction that takes place in the kinetic regime, the rate reaction constant was selected as the main kinetic parameter in the comparison investigation on photocatalytic efficiency of dye removal. The benefit of using rate constants in this investigation was the elimination of adsorption influence that potentially occurs.

The calculated photocatalytic apparent degradation rate constant, k_{app} and the linear regression coefficients, R^2, for the ODT photodegradation of all samples are given in Fig. 1 and Table 1. All samples in both MB/RhB photodegradation reactions mostly followed the pseudo first-order reaction of the L-H kinetic model. High values of linear regression coefficients indicated that the photocatalytic reactions of all studied samples were well fitted with the suggested model, despite the difference in the component ratio, Table 1.

The lowest value of the rate constant in MB photodegradation reaction was detected for the 0%-100ºC and 0%-500ºC samples that additionally indicated the lowest photocatalytic efficiency when compared to the photocatalysts with TiO_2-loading (Fig. 1 (a,b)). Determination of kinetic parameters for photocatalysts synthesized with different TiO_2 content (1%, 2% and 3%) revealed that increasing the TiO_2 amount had a positive effect on photocatalytic performance. However, the experimental data of calcined samples in the MB photodegradation reaction deviated from the assumed kinetic model for the pseudo-first order reaction in the measured range of UV exposure, and followed the proposed kinetic model only at the beginning of the UV reaction. It can be suggested that longer UV exposure initiated a change in the reaction mechanism, which was reflected in the appearance of a “knee” (break) in the dependence diagrams of the mentioned samples, Fig. 1b). These discrepancies correlated with

Table 1. Kinetic parameters for the pseudo-first reaction order.

	MB photodegradation		RhB photodegradation	
Samples	R^2	$k_{app}(min^{-1})$	R^2	$k_{app}(min^{-1})$
0%-100ºC	0.8221	0.0008	0.674	0.0001
1% -100ºC	0.9740	0.0029	0.988	0.0026
2% -100ºC	0.9960	0.0079	0.996	0.0035
3% -100ºC	0.9917	0.0090	0.996	0.0047
0% -500ºC	0.804	0.0021	0.9014	0.0048
1% -500ºC	0.9787	0.0304	0.9906	0.0028
2%-500ºC	0.9655	0.0279	0.9629	0.0023
3% -500ºC	1	0.055	0.9547	0.0020
100%-100ºC	0.8699	0.036	0.9572	0.0259
100%-500ºC	0.9148	0.0364	0.9778	0.0061

the results of the photocatalytic efficiency of the MB degradation of these samples [4, 18]. It was noticed that at mentioned shorter times of UV exposure, the photodegradation efficiency reached almost the maximum, after which a steady reaction regime was achieved and a plateau appeared in all calcined samples. Furthermore, the results indicated that calcined samples in MB photodegration reactions followed the Langmuir-Hinshelwood kinetic model and that the degradation was a pseudo-first order reaction, which, however, most likely ends at shorter UV exposure times. According to the theory of the photocatalytic reaction process, after the reaction is initiated by photons, the final product is desorbed from the surface of the photocatalyst and transferred from the surface to the fluid mass by interfacial diffusion [17].

Kinetic investigation of the RhB photodegradation reaction suggested good correlation of the experimental results with the theoretical settings and revealed that all photocatalysts followed to the Langmuir-Hinshelwood model as a pseudo-first order reaction (Fig. 1 (c,d)). The calculated data of the correlation coefficient and

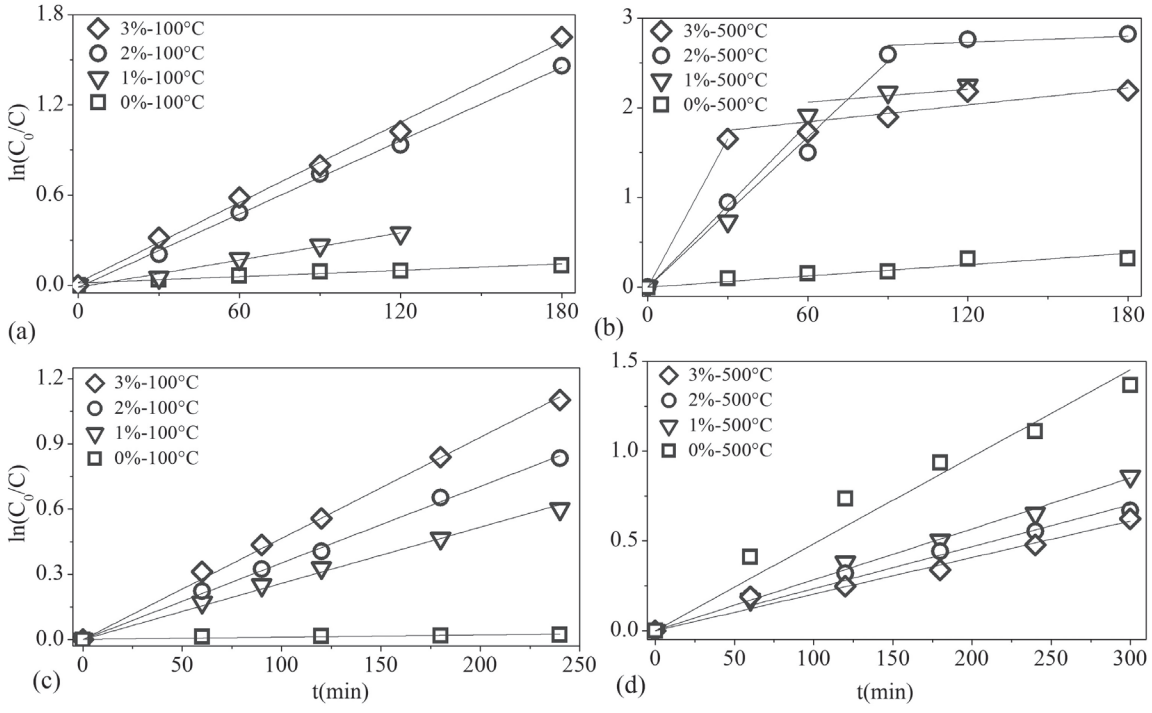

Fig. 1. Pseudo-first order kinetics: a) 100ºC samples MB-UV irradiation; b) 500ºC samples MB-UV irradiation; c) 100ºC samples RhB-UV irradiation and d) 500ºC samples RhB-UV-UV irradiation.

the rate constant of the RhB photocatalytic reaction for all samples are shown in Table 1. From the analysis of kinetic parameters the influence of the TiO_2-loading on photocatalytic performance was observed. It was noticed that with the increase of the TiO_2-loading amount there was an increase in the value of the constant rate of chemical reaction, which indicated improved photocatalytic performance and better photocatalytic efficiency of RhB degradation (Fig. 1c). On the contrary, when observing the kinetic parameters of the calcined samples, it was detected that the rate constant decreased with the increase of the TiO_2-loading. This behavior can be explained by the textural characterization and phase composition [4, 8, 18] of calcined samples: higher amount of larger mesopores resulting in better active center accessibility and higher amount of photocatalytic active, non-stochiometric ZnAl(O) mixed oxides phase following this order: 0%-500ºC>1%-500ºC>2%-500ºC>3%-500ºC. Nevertheless, all calcined samples showed high photocatalytic RhB removal efficiency.

This kinetic investigation confirmed that the mechanism of ODT photocatalytic reactions follow Langmuir-Hinshelwood kinetic model for all studied photocatalysts.

The analysis showed that the rate of the photocatalytic reaction was influenced by the nature of the active sites. This can be supported by the assumptions that follow the L-H model: (i) the amount of the adsorption sites on the surface of the photocatalysts is limited; (ii) only monolayered adsorption is possible with one molecule per active site; (iii) adsorption on the surface is reversable; (iv) catalysts' surface is homogeneous; (v) the adsorb molecule do not interact [27, 28].

Artificial Neural Network Results

The performance result of ANN model for the efficiency of ODT degradation is shown in the Fig. 2. It shows the mean squared error (MSE) variation for number of hidden nodes and type of activation function used for testing data. It can be seen that the MSE decreased up to 8 hidden neurons for both simulated ANN models. Further increase of hidden neurons number results in better predictive capacity of ANN model with logsig activation function as MSE continue to decrease. In the case of tansig activation function, MSE of model network increased. According to the MSE values better prediction are achieved with log sig activation function, as this network has smaller error values.

Coefficient of determination for the efficiency of ODT degradation was in range between 0.753 (single neuron) and 0.975 (11 neurons) for ANN with tansing activation function. After 11 neurons in hidden layer, the drop in R^2 values was registered. Moreover, in the case of ANN with logsig activation function, coefficient of determination increased gradually up to the number of 15 neurons in hidden layer. Further increase of neuron number above 15 resulted in decrease of R^2 (data not shown). These comparative results showed that the ANN with logsig activation function yields higher accuracy in the case of the efficiency of ODT degradation. So, in this case the network with configuration 4-15-1 and logsig activation function was selected.

After training networks with a number of hidden neurons ranging from 1 to 15 (Fig. 3), the optimal activation function was tansig for the photodegradation rate constant data. Networks with a smaller number of hidden neurons had the lowest accuracy, adding additional neurons to the hidden layer improved the prediction of rate constant in the decomposition reaction.

The increase of neurons number in ANN with logsig activation function did not improve network predictions, as the best results were achieved for 13 neurons, R^2 and MSE were 0.746 and 0.0386, respectively. The optimal topology was determined to be a three-layer feed-forward ANN with 3 input neurons and 10 hidden neurons, 3-10-1. In this case (tansig activation function) the R^2 and MSE were 0.982 and 0.0027, respectively.

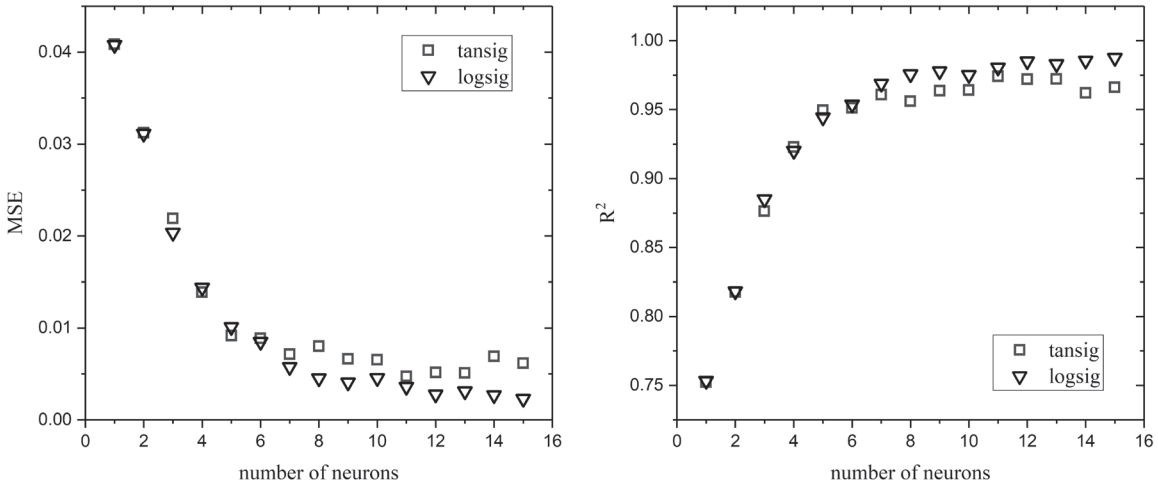

Fig. 2. Relationship between MSE (left), R^2 (right) and number of hidden layer neurons for the efficiency of ODT degradation.

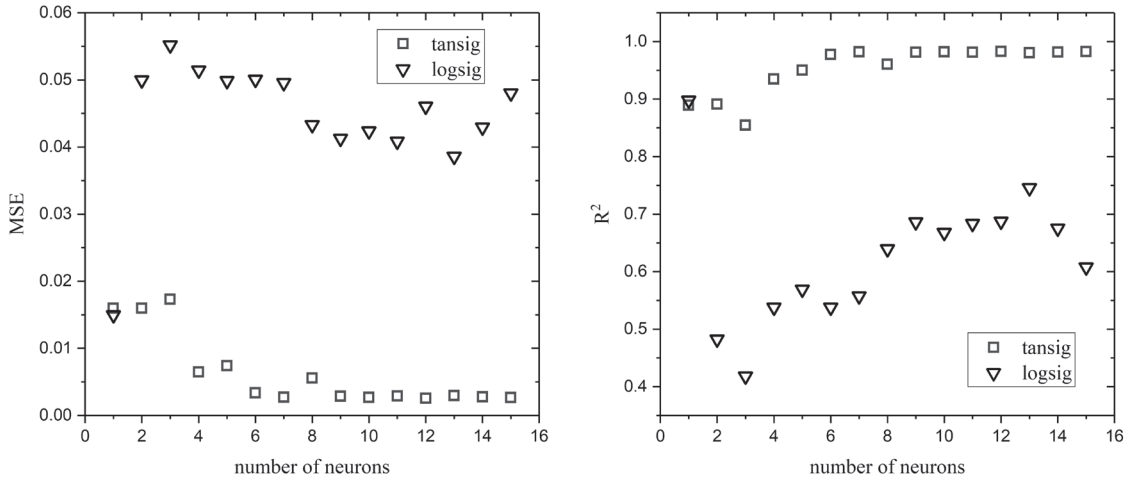

Fig. 3. Relationship between MSE (left), R^2 (right) and number of hidden layer neuron for the photodegradation rate constant.

Fig. 4. shows a comparison between experimental (the efficiency of ODT degradation and photodegradation rate constant) values and predicted values using the ANN model.

The quality of linear regression model (intercept set at 0) was evaluated by the Pearson correlation coefficient (r) and coefficient of determination (R^2) [23]. The values of r for the efficiency of ODT degradation and photodegradation rate constant data, 0.998 and 0.961 respectively, showed strong positive relation between ANN predicted permeation flux values and experimental values. Furthermore, the values of R^2 revealed good linear fitting between ANN predicted permeation flux values and experimental values with model signifying that less than 1% of the total variation cannot be explained by linear model for the efficiency of ODT degradation (R^2 value 0.998). For the R^2 value 0.961 around 4% of the total variation cannot be explained by linear model.

The relative importance (RI) of each input is presented in Fig. 5. The TiO_2-loading onto LDH had the highest relative contribution (around 43%) on the outputs for the efficiency of ODT degradation (Fig.5.left). The reaction time had relative importance of 23%, while organic dye type and temperature of thermal treatment had similar importance values, 18% and 16%, respectively.

The ANN trained for the prediction of photodegradation rate constant importance Fig. 5 right) also had the highest relative contribution of TiO_2-loading onto LDH (around 53%), whereas organic dye type and temperature of thermal treatment had 26% and 21% importance, respectively. It can be summarized that in both neural networks the TiO_2-loading onto LDH (input 3) presented the largest relative contribution. These results are in good correlation with the previous experimental studies, where it was determined that the photocatalytic active phases, as well as the content

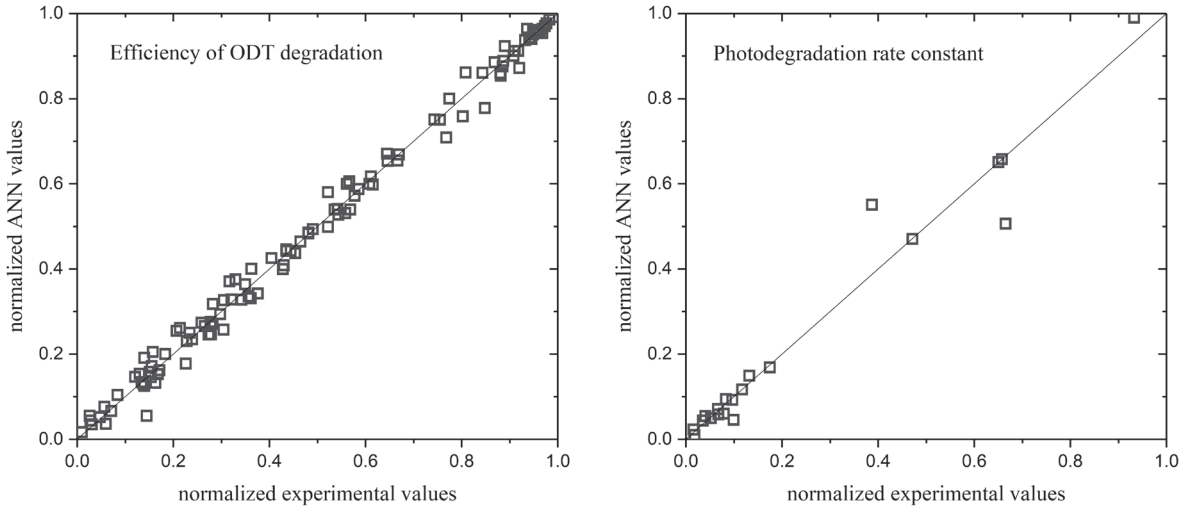

Fig. 4. Normalized experimental values versus ANN predictions for the efficiency of ODT degradation (left) and photodegradation rate constant (right).

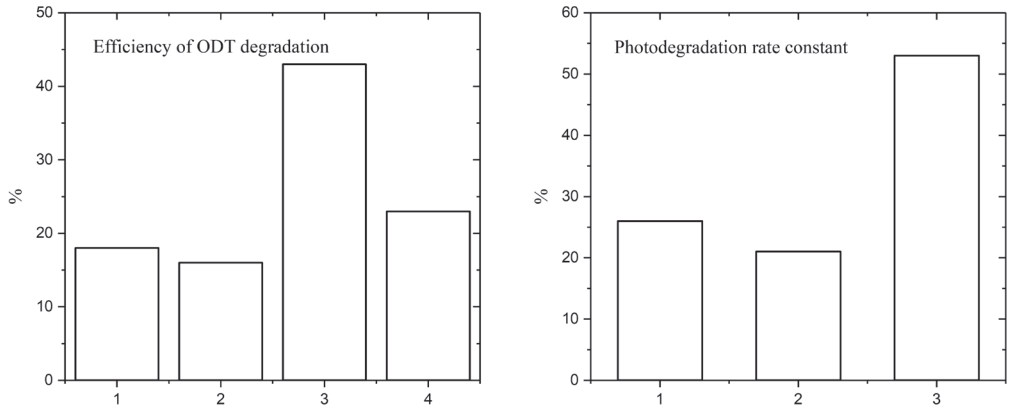

Fig. 5. Relative importance of input variables (1-organic dye type, 2 - temperature of thermal treatment, 3 - loading onto LDH and 4 - reaction time).

of TiO_2 had a significant effect on the photocatalytic efficiency in both ODT removal reactions [4, 8, 18]. High efficiency originates from the interaction of TiO_2 with LDHs derived materials and from the formation of photocatalytic active semiconductor oxides.

Conclusions

An artificial neural network model was developed to predict the photocatalytic performance of TiO_2–LDH based photocatalysts in the cationic dye removal processes. The kinetic investigation revealed high values of linear regression coefficients confirming that the mechanism of MB/RhB photocatalytic reactions follow Langmuir-Hinshelwood kinetic model for all studied photocatalysts, despite the difference in the component ratio. The kinetic studies additionally suggested that the rate of the photocatalytic reaction was influenced by the nature of the active sites. The Artificial neural network model was employed to investigate the importance of each input variable and the optimal topology was determined to be a three-layer feed-forward ANN with 3 input neurons and 10 hidden neurons, 3-10-1. It was concluded that in both MB/RhB removal processes and in both neural networks engaged the largest relative contribution was the amount of TiO_2-loading among all the variables. The use of ANN as statistical tool enable the prediction of the photocatalytic MB/RhB removal over synthesized TiO_2–ZnAl-LDH based photocatalysts. Predicted results were in good agreement with experiments and showed a significant increase of efficiency when TiO_2-loading and exposed surface area increased. This investigation strongly suggests that ANN modeling is an effective and simple approach to successful description of complex photocatalytic removal processes, where the employed operational variables could trigger a combined effect, within the range of experimental conditions investigated. Therefore, this technique has proved to have potential in heterogeneous processes modeling, additionally contributing to the design, scale-up and industrial application of water and wastewater treatment processes.

Acknowledgments

The financial support from the Provincial Secretariat for Higher Education and Scientific Research (Contract No. 142-451-2341/2021-01/02) is gratefully acknowledged.

Conflict of Interest

The authors declare no conflict of interest

References

1. DAS L., MAITY U., BASU J. K. The photocatalytic degradation of carbamazepine and prediction by artificial neural networks. Process Safety and Environmental Protection, **92**, 888, **2014**.
2. NAWAZ A., KHAN A., ALI N., MAO P., GAO X., ALI N., BILAL M., KHAN H. Synthesis of ternary-based visible light nano-photocatalyst for decontamination of organic dyes-loaded wastewater. Chemosphere, **289**, 133121, **2022**.
3. WANG W., WU X., LONG S. Optimizing the Methylene Blue Removal from Aqueous Solution Using Pomelo Peel Based Biochar Assisted by RSM and ANN-PSO. Polish Journal of Environmental Studies, **31** (1), 1, **2022**.
4. HADNADJEV-KOSTIC M., VULIC T., MARINKOVIC-NEDUCIN R., LONCAREVIC D., DOSTANIC J., MARKOV S., JOVANOVIC D. Photo-induced properties of photocatalysts: A study on the modified structural, optical and textural properties of TiO_2-ZnAl layered double hydroxide based materials. Journal of Cleaner Production, **164**, 1, **2017**.
5. KUMARAN V., SUDHAGAR P, KONGA A. K., PONNIAH G. Photocatalytic Degradation of Synthetic Organic Reactive Dye Wastewater Using GO-TiO_2 Nanocomposite. Polish Journal of Environmental Studies, **29** (2), 1683, **2020**.

6. DHIMAN N., MARKANDEYA, SINGH A., VERMA N. K., AJARIA N., PATNAIK S. Statistical optimization and artificial neural network modeling for acridine orange dye degradation using in-situ synthesized polymer capped ZnO nanoparticles. Journal of Colloid and Interface Science, **493**, 295, **2017**.
7. MADDU A., MELIAFATMAH R., RUSTAMI E. Enhancing Photocatalytic Degradation of Methylene Blue Using ZnO/Carbon Dots Nanocomposite Derived From Coffee Grounds. Polish Journal of Environmental Studies, **30** (1), 273, **2021**.
8. HADNADJEV-KOSTIC M., VULIC T., MARINKOVIC-NEDUCIN R. Solar light induced rhodamine B degradation assisted by TiO2–Zn–Al LDH based photocatalysts. Advanced Powder Technology, **25** (5), 1624, **2014**.
9. PRASAD C., TANG H., LIU Q. Q., ZULFIQAR S., SHAH S., BAHADUR I. An overview of semiconductors/layered double hydroxides composites: Properties, synthesis, photocatalytic and photoelectrochemical applications. Journal of Molecular Liquids, **289**, 111114, **2019**.
10. CAVANI F., TRIFIRO F., VACCARI A. Hydrotalcite-type anionic clays: Preparation, properties and applications. Catalysis Today, **11** (2), 173, **1991**.
11. ZHANG R., AI Y., LU Z. Application of Multifunctional Layered Double Hydroxides for Removing Environmental Pollutants: Recent Experimental and Theoretical Progress. Journal of Environmental Chemical Engineering, **8**, 103908, **2020**.
12. JIANG Z., HU J., ZHANG X., ZHAO Y., FAN X., ZHONG S., ZHANG H., YU X. A generalized predictive model for TiO_2–Catalyzed photo-degradation rate constants of water contaminants through artificial neural network. Environmental Research, **187**, 109697, **2020**.
13. ZHOU C., WANG Q., ZHOU C. Photocatalytic degradation of antibiotics by molecular assembly porous carbon nitride: Activity studies and artificial neural networks modeling. Chemical Physics Letters, **750**, 137479, **2020**.
14. FRONTISTIS Z., DASKALAKI V. M., HAPESHI E., DROSOU C., FATTA-KASSINOS D., XEKOUKOULOTAKIS N. P., MANTZAVINOS D. Photocatalytic (UV-A/TiO_2) degradation of 17α-ethynylestradiol in environmental matrices: Experimental studies and artificial neural network modeling. Journal of Photochemistry and Photobiology A: Chemistry, **240**, 33, **2012**.
15. FIDALGO A., LETICHEVSKY S., SANTOS B. F. Assessment of TiO_2 band gap from structural parameters using artificial neural networks. Journal of Photochemistry & Photobiology, A: Chemistry, **405**, 112870, **2021**.
16. DUTTA S., PARSONS S.A., BHATTACHARJEE C., BANDHYOPADHYAY S., DATTA S. Development of an artificial neural network model for adsorption and photocatalysis of reactive dye on TiO2 surface. Expert Systems with Applications, **37**, 8634, **2010**.
17. REDDY B.S., MAURYA A.K., NARAYANA P.L., KHADHEER PASHA S.K., REDDY M.R., HATSHAN M.R., DARWISH N.M., KORI S.A., CHO K.-K., REDDY N.S. Knowledge extraction of sonophotocatalytic treatment for acid blue 113 dye removal by artificial neural networks. Environmental Research, **204**, 112359, **2022**.
18. HADNADJEV-KOSTIC M., VULIC T., RANOGAJEC J., MARINKOVIC-NEDUCIN R., RADOSAVLJEVIC-MIHAJLOVIC A. Thermal and photocatalytic behavior of Ti/LDH nanocomposites. Journal of Thermal Analysis and Calorimetry, **111,** 1155, **2013**.
19. BARAN W., ADAMEK E., MAKOWSKI A. The influence of selected parameters on the photocatalytic degradation of azo-dyes in the presence of TiO_2 aqueous suspension. Chemical Engineering Journal, **145**, 242, **2008**.
20. KURIECHEN S.K., MURUGESAN S., RAJ S.P., MARUTHAMUTHU P. Visible light assisted photocatalytic mineralization of Reactive Red 180 using colloidal TiO_2 and oxone. Chemical Engineering Journal, **174**, 530, **2011**.
21. CORBATÓN-BÁGUENA M.-J., VINCENT-VELA M.-C., GOZÁLVEZ-ZAFRILLA J.-M., ÁLVAREZ-BLANCO S., LORA-GARCÍA J., CATALÁN-MARTÍNEZ D. Comparison between artificial neural networks and Hermia's models to assess ultrafiltration performance. Separation and Purification Technology, **170**, 434, **2016**.
22. ASGHARI M., DASHTI A., REZAKAZEMI M., JOKAR E., HALAKOEI H., Application of neural networks in membrane separation. Reviews in Chemical Engineering, **36** (2), 265, **2020**.
23. JOKIĆ A., NIKOLIĆ N., LUKIĆ N., GRAHOVAC J., DODIĆ J., RONČEVIĆ Z., ŠEREŠ Z. Dynamic Modeling of Streptomyces hygroscopicus Fermentation Broth Microfiltration by Artificial Neural Networks. Periodica Polytechnica Chemical Engineering, **63** (4), 541, **2019**.
24. BAYAR S., DEMIR I., ENGIN G. O. Modeling leaching behavior of solidified wastes using back-propagation neural networks. Ecotoxicology and Environmental Safety, **72** (3), 843, **2009**.
25. WINICZENKO R., GÓRNICKI K., KALETA A., JANASZEK-MAŃKOWSKA M. Optimisation of ANN topology for predicting the rehydrated apple cubes colour change using RSM and GA. Neural Computing and Applications, **30** (6), 1795, **2016**.
26. CHELLAM S. Artificial neural network model for transient crossflow microfiltration of polydispersed suspensions. Journal of Membrane Science, **258** (1), 35, **2005**.
27. ARMENISE S., GARCIA-BORDEJE E., VALVERDE J.L., ROMEO E., MONZON A. A Langmuir–Hinshelwood approach to the kinetic modelling of catalytic ammonia decomposition in an integral reactor. Physical Chemistry Chemical Physics, **15**, 12104, **2013**.
28. KHATAEE A.R., FATHINIA M., ABER S. Kinetic modeling of liquid phase photocatalysis on supported TiO_2 Nanoparticles in a rectangular flat-plate photoreactor. Industrial & Engineering Chemistry Research, **49**, 12358, **2010**.